

Article

Complexity of Electron Injection Dynamics and Light Soaking Effects in Efficient Dyes for Modern DSSC

Adam Glinka *, Jacek Kubicki  and Marcin Ziółek * 

Quantum Electronics Laboratory, Faculty of Physics, Adam Mickiewicz University in Poznań, Uniwersytetu Poznańskiego 2, 61-614 Poznań, Poland; jacek.kubicki@amu.edu.pl

* Correspondence: adam.glinka@amu.edu.pl (A.G.); marziol@amu.edu.pl (M.Z.)

Abstract: Electron transfer dynamics in dye sensitized solar cells (DSSCs) employing triphenylamine Y123 dye were investigated by means of femtosecond broadband transient absorption spectroscopy in the visible and mid-IR range of detection. The electron injection process to the titania conduction band was found to appear biphasically with the time constant of the first component within 350 fs and that of the second component between 80 and 95 ps. Subsequently, the effects of continuous irradiation on the ultrafast and fast electron transfer processes were studied in the systems comprising Y123 dye or carbazole MK2 dye in combination with cobalt- or copper-based redox mediators: [Co(bpy)₃](B(CN)₄)_{2/3} (bpy = 2,2'-bipyridine) or [Cu(tmby)₂](TFSI)_{1/2} (tmby = 4,4',6,6' tetramethyl-2,2'-bipyridine, TFSI = bis(trifluoromethane)sulfonamide). We have found that the steady-state illumination led to acceleration of the electron injection process due to the lowering of titania conduction band edge energy. Moreover, we have observed that the back electron transfer to the oxidized dye was suppressed. These changes in the initial (up to 3 ns) charge separation efficiency were directly correlated with the photocurrent enhancement.

Keywords: dye sensitized solar cell; electron injection; light soaking; triphenylamine dye; carbazole dye; cobalt complex; copper complex; ultrafast VIS spectroscopy; ultrafast mid-IR spectroscopy



Citation: Glinka, A.; Kubicki, J.; Ziółek, M. Complexity of Electron Injection Dynamics and Light Soaking Effects in Efficient Dyes for Modern DSSC. *Energies* **2021**, *14*, 407. <https://doi.org/10.3390/en14020407>

Received: 12 December 2020

Accepted: 11 January 2021

Published: 13 January 2021

Publisher's Note: MDPI stays neutral with regard to jurisdictional claims in published maps and institutional affiliations.



Copyright: © 2021 by the authors. Licensee MDPI, Basel, Switzerland. This article is an open access article distributed under the terms and conditions of the Creative Commons Attribution (CC BY) license (<https://creativecommons.org/licenses/by/4.0/>).

1. Introduction

Dye sensitized solar cells (DSSCs) have been much improved since the breakthrough achieved by O'Regan and Graetzel in 1991 [1]. Although DSSC have been recently outperformed by other emerging photovoltaic technologies (including perovskite [2], quantum dot solar cells [3], and organic photovoltaics [4]) in terms of power conversion efficiency (PCE) in full sunlight conditions, they are experiencing a renaissance and have attracted interest again, thanks to their superior performance in low ambient light conditions [5–7]. Thus, such cells enable powering of the novel class of electronic devices networked on the Internet of Things (IoT) [5]. In the pursuit of more efficient, stable, environmentally friendly, and cheap DSSC systems, a great deal of widely used materials and compounds have been replaced by novel counterparts, setting new standards. In particular, the introduction of fully organic D-π-A dyes [8–11] replacing ruthenium complexes [12] permitted bypassing a problem of low abundance and high price of this element as well as the issue of relatively low extinction coefficients of its coordination compounds. Another milestone achievement has been the replacement of iodide/triiodide (I⁻/I₃⁻) redox couple by new generation of coordination compounds of cobalt (Co³⁺/Co²⁺) [9] and more environmentally friendly copper (Cu²⁺/Cu⁺) [13–15], which allowed achieving over 1.1 V open circuit voltages (V_{OC}) in highly efficient DSSCs.

Thanks to the advances in new compounds and materials design, the highest achieved PCEs has been pushed up to ~14% [16,17] at full sunlight and 32–34% [5,18] in ambient light conditions. At the same time, the above-mentioned advances have raised fundamental questions on the operation of systems comprising the state-of-the-art cell components. Although

the number of studies focused on triphenylamine (TPA) dyes in combination with transition metals coordination compounds as redox mediators is relatively high [10,15,16,19], only a few authors have brought up a topic of ultrafast electron transfer dynamics of the benchmark TPA dye: 3-{6-[4-[bis(2',4'-dihexyloxybiphenyl-4-yl) amino-]phenyl]-4,4-dihexyl-cyclopenta-[2,1-b:3,4-b'] dithiophene-2-yl]-2-cyanoacrylic acid coded as Y123 (or its popular counterpart coded as LEG4) [20,21], Supplementary Scheme S1A. In particular, no detailed information has been published on the examination of the excited state dynamics of Y123 interacting with mesoporous titania in broad visible light spectrum. This issue should be examined, especially in light of recent advances on new, more complex and highly efficient TPA dyes [17,22–24]. It is especially important to establish whether the dynamics of electron injection in the fully operating solar cells occurs on the ultrafast time scale up to single ps (like for many organic dyes for DSSC), or extends into much longer time scales, e.g., for some ruthenium compounds [25,26]. According to our knowledge, so far there have been only two reports about the electron injection dynamics for Y123. In the first report the process occurring within about 2 ps was detected using femtosecond diffuse reflectance spectroscopy [21]. In the second one, the contribution of the electron injection time constant of 12 ps was reported in the inert electrolyte, using the picosecond time-resolved transient absorption (TA) spectroscopy [20]. Surprisingly, this time constant has been extended to 25 ps in the samples with a solid state Cu-based electrolyte [20]. It should be noted that in both the above-mentioned papers, the electron injection time constant determination has been based on the transient absorption kinetics at a single probe wavelength in the visible range. Moreover, in the context of suggestions reported on the possibility of direct interfacial electron transfer [27] between the LEG4 dye ground state and the conduction band of titania, based on the theoretical studies [28], a comprehensive experimental study was needed to verify if this process took place. If it does take place and is thoroughly characterized, it could help bypass the most significant potential loss in the state of the art DSSCs, which is caused by the electron injection process [7,23], so it should not be disregarded.

Thanks to the advances in new compounds and materials design, the highest achieved PCEs has been pushed up to ~14% [16,17] at full sunlight and 32–34% [5,18] in ambient light conditions. At the same time, the above-mentioned advances have raised fundamental questions on the operation of systems comprising the state-of-the-art cell components. Although the number of studies focused on triphenylamine (TPA) dyes in combination with transition metals coordination compounds as redox mediators is relatively high [10,15,16,19], only a few authors have brought up a topic of ultrafast electron transfer dynamics of the benchmark TPA dye: 3-{6-[4-[bis(2',4'-dihexyloxybiphenyl-4-yl) amino-]phenyl]-4,4-dihexyl-cyclopenta-[2,1-b:3,4-b'] dithiophene-2-yl]-2-cyanoacrylic acid coded as Y123 (or its popular counterpart coded as LEG4) [20,21], Supplementary Scheme S1A. In particular, no detailed information has been published on the examination of the excited state dynamics of Y123 interacting with mesoporous titania in broad visible light spectrum. This issue should be examined, especially in light of recent advances on new, more complex and highly efficient TPA dyes [17,22–24]. It is especially important to establish whether the dynamics of electron injection in the fully operating solar cells occurs on the ultrafast time scale up to single ps (like for many organic dyes for DSSC), or extends into much longer time scales, e.g., for some ruthenium compounds [25,26]. According to our knowledge, so far there have been only two reports about the electron injection dynamics for Y123. In the first report the process occurring within about 2 ps was detected using femtosecond diffuse reflectance spectroscopy [21]. In the second one, the contribution of the electron injection time constant of 12 ps was reported in the inert electrolyte, using the picosecond time-resolved transient absorption (TA) spectroscopy [20]. Surprisingly, this time constant has been extended to 25 ps in the samples with a solid state Cu-based electrolyte [20]. It should be noted that in both the above-mentioned papers, the electron injection time constant determination has been based on the transient absorption kinetics at a single probe wavelength in the visible range. Moreover, in the context of suggestions reported on

the possibility of direct interfacial electron transfer [27] between the LEG4 dye ground state and the conduction band of titania, based on the theoretical studies [28], a comprehensive experimental study was needed to verify if this process took place. If it does take place and is thoroughly characterized, it could help bypass the most significant potential loss in the state of the art DSSCs, which is caused by the electron injection process [7,23], so it should not be disregarded.

Thus, in this work, we focused on analysis of the excited state dynamics and charge transfer processes occurring in DSSC systems comprising Y123 dye. We aimed at answering the questions about possible modes and solving the controversies (vide infra) about the dynamics of electron injection. To do this, we used femtosecond transient absorption in the broad visible spectral range as well as femtosecond transient absorption in the mid-IR range. To achieve better understanding of the processes observed, the transient absorption kinetics at many wavelengths were analyzed simultaneously by means of the global fit. Transient absorption techniques in both visible and IR ranges were used to study the electron injection dynamics in DSSCs since the initial systems with ruthenium compounds had already been extensively studied [26,29–31]. These techniques have been frequently used for DSSC with ruthenium and other organic dyes, as reviewed, e.g., in [25,32–36]. Moreover, our study was conducted on full operational DSSC samples as well as half cells based on sapphire substrates (transparent in mid-IR), however preserving all the same conditions relevant for studied processes. The dye cells used in this study were also subjected to constant illumination to study the changes that occur in the systems within the first hour of operation. In this way we could not only evaluate the proposed charge transfer model, but also reveal some new insights into the way that charge transfer phenomena in DSSCs change, due to the so called light soaking effects. They are commonly observed in DSSC systems [37–40] and have been usually assigned to the shifts of the conduction band edge [37,38] which could be caused by light induced changes in equilibrium of positively charged ions (Li^+ , H^+) and Lewis base (predominantly *tert*-butylpyridine—TBP) on the semiconductor/electrolyte interface [40]. Although the light soaking effect for DSSCs is very important, its detailed impact on electron injection and recombination dynamics in the studied systems has not been reported so far.

Besides the Y123 based cells, we used well-described systems based on carbazole MK2 dye (Supplementary Scheme S1B), extensively studied by our group for the last few years [41–45]. Both dyes were studied in combination with $[\text{Co}(\text{bpy})_3](\text{B}(\text{CN})_4)_{2/3}$ ($\text{bpy} = 2,2'$ -bipyridine) [9] and $[\text{Cu}(\text{tmby})_2](\text{TFSI})_{1/2}$ ($\text{tmby} = 4,4',6,6'$ tetramethyl-2,2'-bipyridine, TFSI = bis(trifluoromethane)sulfonamide) [15], providing new insights into the dynamics of electron separation and recombination in Y123 and their impact on photocurrent generation.

2. Materials and Methods

2.1. Device Fabrication

Unless otherwise stated, all the chemicals were purchased from Sigma-Aldrich (Saint Louis, MO, USA) and used without additional purification. The FTO (fluorine doped tin oxide) coated glass sheet (Sigma-Aldrich, Saint Louis, MO, USA, 2.2 mm thick, $13 \Omega \text{ sq}^{-1}$) was cleaned, the mesoporous titania layers (including pre- and post- TiCl_4 treatment) were deposited and the DSSCs were fabricated according to the procedures described elsewhere [45]. A layer of mesoporous titania of 2–3 μm in thickness, without a scattering film, was prepared by screen-printing technique, to provide sufficient light transmission for optical absorption measurements. The screen-printable 28–31 nm titania nanoparticles containing paste (DN-GPS-30TS) were provided by Dyenamo, Sweden. The compositions of solutions for titania sensitization were as follows: for Y123 (Dyenamo, Stockholm, Sweden) sensitized solar cells: 0.1 mM dye solution with 0.2 mM addition of cheno-deoxycholic acid (CDCA) in acetonitrile (ACN) and *tert*-butanol (*tert*-BuOH) 1:1 mixture, while for MK2 sensitized cells a 0.2 mM dye solution in toluene (TOL) was used. To some of the MK2 cells, 0.1 mM of CDCA was added. The electrolyte solution compositions were as follows:

Co-based—0.25 M $[\text{Co}(\text{bpy})_3](\text{B}(\text{CN})_4)_2$, 0.035 M $[\text{Co}(\text{bpy})_3](\text{B}(\text{CN})_4)_3$, 0.1 M LiClO_4 and 0.5 M TBP in ACN; Cu-based—0.2 M $[\text{Cu}(\text{tmby})_2](\text{TFSI})$, 0.04 M $[\text{Cu}(\text{tmby})_2](\text{TFSI})_2$, 0.1 M LiTFSI , 0.6 M TBP in ACN. In some indicated control cells, the electrolytes without TBP were used. Platinized counter electrodes for Co-based and poly-3,4 ethylenedioxythiophene (PEDOT) coated ones for Cu-based electrolyte mediated solar cells were prepared according to methods specified elsewhere [46].

Titania substrates for half-cells for mid-IR optical measurements were prepared according to the same procedures as for full DSSCs, but on 3 mm thick sapphire windows (Thorlabs) to provide transparency for mid-IR light. Sensitized titania substrates were sandwiched with blank sapphire window, with a 5 μL drop of the electrolyte inside and tightened with a gasket cut from Parafilm[®] inside a 3D printed frame presented in Supplementary Figure S1A.

2.2. Device Characterization

Steady state absorption spectra of sensitized or bare photoanodes were measured using a JASCO (Tokio, Japan) V-770 UV-VIS-NIR spectrophotometer equipped with 150 mm integrating sphere (LN-925). Current-voltage and incident photon to current efficiency (IPCE) spectra measurements were performed on the system coupling an Metrohm Autolab (Utrecht, Netherlands) M101 potentiostat and a photoelectric spectrometer (Instytut Fotonowy, Kraków, Poland) comprising a 150 W Xe lamp with an AM 1.5 G spectral filter adjusted to 100 mW cm^{-2} using a calibration cell (ABET-Technologies, Milford, CT, USA, model 15151).

The transient absorption (TA) systems (UV-VIS Helios spectrometer, Ultrafast Systems, Sarasota, FL, USA), and mid-IR PhaseTech Spectroscopy, Inc., Madison, WI, USA), 2D Quick Transient spectrometer, coupled with Spectra-Physics (Santa Clara, CA, USA) laser system, have been described in detail formerly [41,47]. The instrument response function (IRF) width was 100–200 fs and 350 fs (FWHM) for VIS and mid-IR experiments, respectively. In broadband VIS experiment, the pump pulse energies were set to different values providing approximately constant signal response for different wavelengths (20 nJ, 70 nJ and 200 nJ translating to 10 $\mu\text{J cm}^{-2}$, 35 $\mu\text{J cm}^{-2}$, and 100 $\mu\text{J cm}^{-2}$, respectively). In the mid-IR experiment, the pump pulse energies were set to 50 nJ, 100 nJ, and 500 nJ, which equals 200 $\mu\text{J cm}^{-2}$, 400 $\mu\text{J cm}^{-2}$, and 2 mJ cm^{-2} energy density. Transient absorption data were analyzed using the Surface Explorer software (Ultrafast Systems, Sarasota, FL, USA).

3. Results and Discussion

3.1. Monitoring Electron Injection in the Cells with Y123

In order to develop the model of charge transfer dynamics in the systems containing Y123 dye sensitized titania nanoparticles, we performed transient absorption measurements for full operational solar cells with Co- and Cu-based electrolytes (see the next section for the photovoltaic parameters of the samples). The data collected in 3 ns time window and 530–850 nm spectral range were analyzed by means of the singular value decomposition using 3 kinetic vectors. Subsequently, to obtain time constants and their wavelength dependent amplitudes (also called the pre-exponential factor spectra), three-exponential global analysis, including the convolution with IRF, was performed. Additionally, the constant offset component was incorporated, to take the residual spectra into account.

To get insight into the dynamics of excited state of Y123, the TA measurements were performed using three different pump wavelengths in the range of the dye's operation spectra. This strategy was chosen taking into account the hypothesis that that different electron injection processes might occur in the system with different contributions, depending on the excitation wavelengths. The range of the dye's operation was determined on the basis of the IPCE spectra shown in Supplementary Figure S1B. The IPCE onset wavelength in Y123 sensitized solar cells is equal to 700 nm and in our semi-transparent electrodes, 10% of the IPCE maximum was already reached at 640 nm. Thus, we have chosen it for the longest pump wavelength. The long wavelength response can be enhanced by the incorporation

of a thicker titania layer supported by scattering nanoparticles coating. However, such a construction of the solar cell does not provide sufficient quality of transient absorption measurements in the transmission mode.

Positive transient absorption signals in the visible light spectral range may originate from photon absorption from the excited electronic state of the dye to higher excited states of dye or may be due to absorption of a new species (e.g., oxidized dye). On the other hand, the negative signals are connected mainly with the ground state depopulation (bleaching) or stimulated emission. The components of transient absorption containing contributions from the decay of S_1 excited state as well as building up the band assigned to the oxidized state (manifested as a negative amplitude of pre-exponential factor) may be assigned to electron injection to the titania conduction band [25,35]. At the same time, the components related to the Y123 ground state recovery and the oxidized state band decay, should be linked to the undesired charge recombination process [48,49]. However, spectral and temporal overlapping of the TA signals originating from different processes, often makes a direct assignment of the obtained components to particular electron transfer processes arduous or even impossible. That is why different experimental approaches are usually required for proper charge transfer model elucidation. Therefore, in this work apart from the ultrafast transient absorption spectroscopy in the visible range, the ultrafast transient absorption spectroscopy in the mid-IR range was applied, which permits direct probing of the population of free electrons in titania conduction band [35,41,47].

Examples of original transient absorption spectra in the visible range for DSSCs with Y123 dye are shown in Supplementary Figure S2, while Figure 1 presents the pre-exponential factor spectra of the components obtained in the global analysis for pump wavelength at 560 nm. ΔA stands for the difference between the absorbances with and without a pump pulse. The spectrum of the fastest (1–2 ps) component contains a negative amplitude (or indentation in the positive amplitude) in the range matching the fluorescence spectrum (see Supplementary Figure S3). That is why this feature may be interpreted as stimulated emission decay. Another important feature of the first component is the positive band with the maximum around 700 nm, which should be related to the transition between S_1 state and one of higher excited electronic states of the dye (see the results in solution in Supplementary Figure S4). Supplementary Figure S5 shows the pre-exponential factor spectra for different pump wavelengths (480 and 640 nm) at pump pulse energies tuned to have similar amplitude of TA signal. With increasing pump wavelength, the peak of the first component is shifted to the blue and approaches a central wavelength of the similar positive band present in the second (10–20 ps) component (Figure 2, the longer the pump wavelength, the smaller the difference between the band maxima of the first and second components). Supplementary Table S1 collects the time constants for all components at three excitation wavelengths.

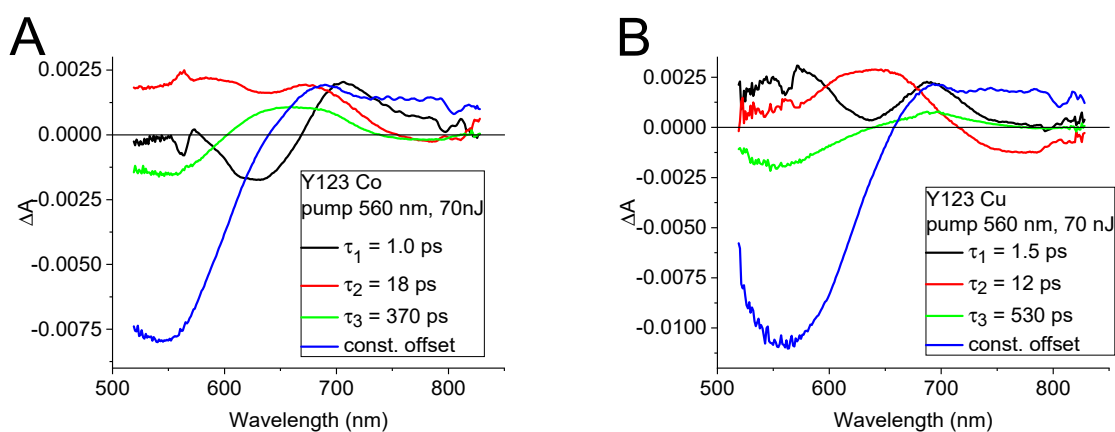


Figure 1. Pre-exponential factor spectra associated with the indicated time constants for a model with a three-exponential function with an offset for DSSC with Y123 dye and (A) cobalt- and (B) copper-based electrolyte for pump wavelength 560 nm.

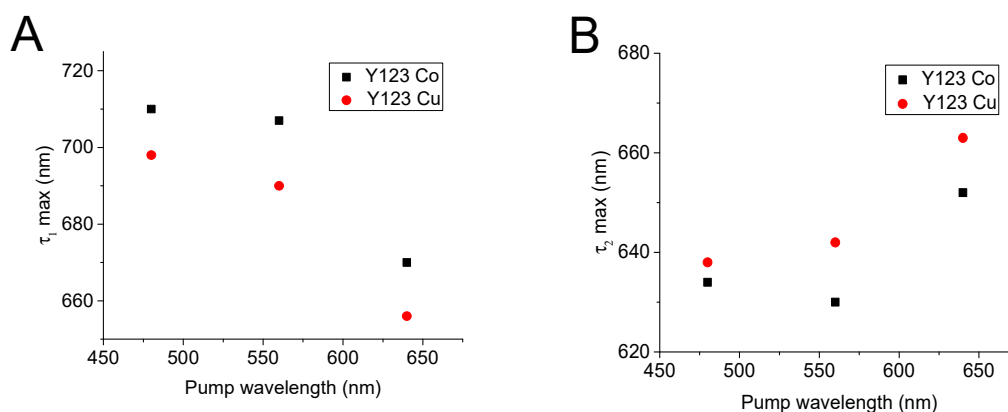


Figure 2. Maxima of the positive band in pre-exponential factor spectra of the (A) first and (B) second component of the global analysis for Y123 solar cells.

The wavelength-dependent amplitude of the second component contains also a negative signal or an indentation in the positive signal in the range between 700 nm and 850 nm, which can be assigned to the stimulated emission and/or to building up of the oxidized state population (the rise of its transient absorption can be visible as the second peak in the photoinduced absorption measurements [46]). For the samples containing a cobalt redox mediator, the positive band in the short wavelength part of the spectra, may be distorted by the residuum of the stimulated emission from hot (Franck–Condon) S_1 state of the dye. Small shifts (~ 10 nm) between the spectra recorded in Co and Cu based electrolytes, observed, e.g., in the positions of bleach bands in Figure 1, the positions of the absorption maxima in Figure 2, and IPCE spectra in Supplementary Figure S1B should be also noticed. These shifts probably originate from the slightly different solvation of the dye in the presence of the two electrolytes and can explain a small difference in the shape of the wavelength dependent spectra of the same transient absorption component for the two electrolytes (Figure 1 and Supplementary Figure S5).

The spectral evolution of the first two components observed with decreasing pump photon energy, indicates that τ_1 time constant can be associated with the hot S_1 state while τ_2 can be associated with a decay of the relaxed S_1 state. Similar behavior can be observed in the global analysis of transient absorption of Y123 in solution (Supplementary Figure S4), for which the second (~ 220 ps) component contains the bleach recovery and excited state decay, and the first (~ 2 ps) constituent exhibits Gaussian-like derivative shape, indicating a band shift typical of the excited state relaxation and solvation. In the presence of titania, both decays (of hot and relaxed S_1 state) must be affected by electron transfer to the semiconductor's conduction band, thus for DSSC samples we can assign the shortening of τ_1 and τ_2 to the process of carrier injection. Even though the TA measurements with detection in visible light were conducted using different pump wavelengths approaching the IPCE spectrum onset as close as possible maintaining reliable TA signal and reasonable pump pulse energy, we did not find any strong evidence for interfacial electron transfer occurring directly from the dye's ground state to the titania conduction band (CB).

The third (370–530 ps) component contains a negative band in the range of steady-state absorption of the dye, so we identify this decay as the dye ground state recovery connected with semiconductor-oxidized dye recombination. In the DSSCs systems studied using this method, the recombination component spectrum should match that of the constant offset (the decay with infinite time constant relative to a temporal range ~ 3 ns of our ultrafast spectrometers), which contains the ground state bleach and oxidized dye spectra [41]. In this case, the third component does not show positive amplitudes in the same range that we have previously assigned to building up of the oxidized dye band, caused by electron

injection (>700 nm). This fact suggests that the electrons may be injected in a time scale beyond the second component and thus may contribute to the third one too.

Therefore, we used time resolved infrared absorption spectroscopy, to directly observe the population of electrons injected to the titania conduction band. The measurements were performed on half-cells on the sapphire window (instead of FTO glass) and are described in the experimental section. The pump wavelength was set to 500 nm and the TA signal was monitored at the central wavelength equal to 4780 nm, away from the Y123 molecular vibrations. Thus, the recorded signal is exclusively proportional to the population of the electrons injected to the titania conduction band.

Figure 3 shows the kinetic traces measured at three different pump pulse energies, together with the fitted functions. Independently of the applied pump pulse energy, the population of electrons injected to the titania conduction band rises biphasically with the first rise in the instantaneous component (within IRF duration of 350 fs) and the second rise between 80 ps and 95 ps. For higher pump pulse energy, a higher value of the second time constant (Supplementary Table S2) is observed. However, the contribution of the second component drops relative to that of the first instantaneous component, with increasing pump pulse energy (Figure 3B). This observation could be explained assuming that higher density of charge injected in titania CB during the first instantaneous process, lifts up the quasi Fermi level, and reduces the driving force for electron transfer. Additionally, at high pump pulse energy, the slower injection is masked by more pronounced fast recombination to oxidized dye, which appears in the 500 nJ kinetics as the fast (<1 ps) decay. In general, the back electron transfer may also contribute to 100 nJ and 50 nJ kinetics, but to a much lower extent. We can also conclude, that in the operational conditions (low pump intensities) the slower component (~ 80 ps) brings the highest contribution.

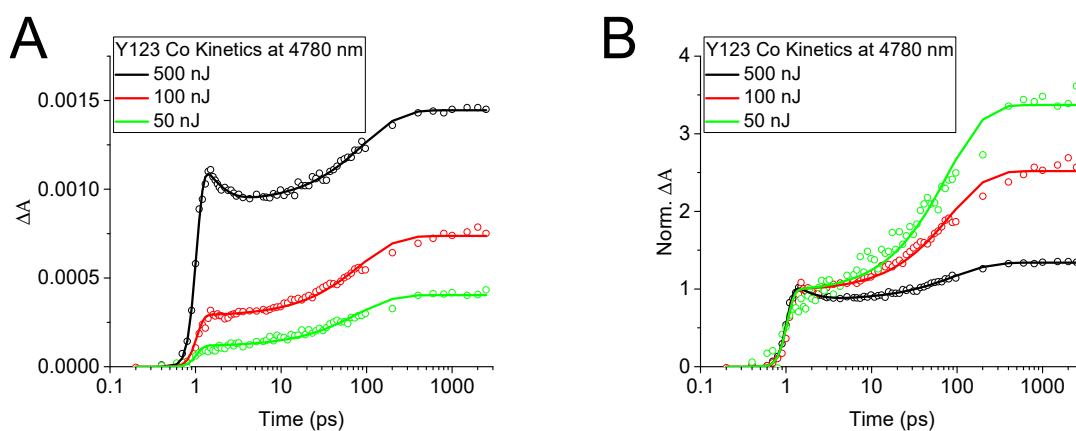


Figure 3. Kinetic traces at 4780 nm for Y123 samples cells with sapphire substrate at different pump intensity (points) with the fitted function (solid lines) (A) as measured and (B) normalized. The time zero was shifted to 1 ps in order to present the time axis in logarithmic scale. The parameters of the fits are given in Supplementary Table S2.

The initial signal magnitude dependence on the pump pulse energy is linear, thus, we can exclude any artifacts originating from two-photon absorption. To exclude other contributions, we performed experiment in the same conditions on the half-cell comprising bare titania without a dye (Supplementary Figure S7) and additionally in the area without titania, to exclude window's, solvent's and redox mediator's contributions. The second measurement did not reveal any signal higher than the noise level. However, the magnitude of the bare titania initial signal made nearly a half of the initial response of Y123 sensitized half-cell. No rise of the signal, but only a decay was revealed. It can be ascribed to the absorption of photons associated with transitions of electrons trapped within the mesoporous titania bandgap, but it must be noted that, in the presence of a dye characterized by a high extinction coefficient (the sensitized photoanode's absorbance was >1.5), competing in pump photons absorption, this contribution can be neglected.

The conclusion that can be drawn from the above experimental evidence is that electron injection into the solar cells sensitized with Y123 dye takes place on several time scales extending from sub-ps or single ps (from the dyes hot excited S_1 Frank–Condon (F-C) state) to about 80 ps (from the relaxed excited state). The contribution of the latter is dominant at low pump pulse energy, so also very likely in the operating 1 Sun conditions. The 80 ps component observed in mid-IR experiments corresponds partially to the second component (10–20 ps) and partially to the third component (370–530 ps) in VIS range. The latter contains also the contribution of electron recombination.

Supplementary Scheme S2 shows the proposed kinetic model of the electron injection taking place in the cells comprising Y123 dye. We believe that our results explain the previous discrepancies in the reported electron injection time constants for this dye: 2 ps in [21] and 12 ps or 25 ps in [20], which lie between the fastest and the slowest electron injection components revealed in this study. Most probably, the above time constants determined from transient absorption kinetics at a single wavelength (690 nm in [21] and 650 nm in two different environments in [20]) contained the specific partial contributions of the injection processes from the hot S_1 and relaxed S_1 states. As we have showed above, the contributions of the hot and relaxed states to the injection process are different at different probing wavelengths in the visible range. Moreover, for the Y123 dye the pre-exponential factor spectra were also slightly spectrally shifted depending on the used electrolyte (Co or Cu based). Therefore, depending on the environment and probing wavelength, the single kinetics can contain different contributions of the fast and slow electron injection components. On the contrary, the approach proposed by us (direct monitoring of electron population in the CB of titania by means of the ultrafast mid-IR spectroscopy accompanied with the broadband analysis in the visible range to assign the observed kinetics components to different states) permits revealing the global picture of the electron injection in the cells comprising Y123 and related dyes.

3.2. Photovoltaic Performance and Continuous Irradiation Effects

The photovoltaic parameters of our solar cell samples are given in Table 1. The performance of DSSCs prepared in this study departs from the highest reported for analogous systems in terms of the photocurrent density (J_{SC}) (7.0, 7.5 and 9.2 mA cm^{-2} vs. 14.6, 15.5 and 15.1 mA cm^{-2} for Y123 $\text{Co}^{3+/2+}(\text{bpy})_3$ [11], Y123 $\text{Cu}^{2+/+}(\text{tmby})_2$ [15] and MK2 $\text{Co}^{3+/2+}(\text{bpy})_3$ [50], respectively) and in terms of the fill factor (FF) (0.57, 0.6 and 0.65 vs. 0.64, 0.7 and 0.75, respectively).

Table 1. Photovoltaic parameters of the studied solar cells (before irradiation)¹.

Cell	PCE [%]	Voc [V]	FF	Jsc [mA cm^{-2}]	Total APCE
Y123 $\text{Co}^{3+/2+}(\text{bpy})_3$	3.8	0.96	0.57	7.03	0.69
error	0.2	0.01	0.02	0.15	0.02
Y123 $\text{Cu}^{2+/+}(\text{tmby})_2$	4.7	1.06	0.60	7.47	0.73
error	0.2	0.01	0.01	0.06	0.01
MK2 $\text{Co}^{3+/2+}(\text{bpy})_3$	5.1	0.85	0.65	9.22	0.71
error	0.2	0.01	0.02	0.11	0.01

¹ PCE, power conversion efficiency; V_{OC} , open circuit voltage; J_{SC} , short circuit photocurrent density; FF, fill factor. Parameters were averaged from at least three devices. Errors were calculated as the standard deviation of the mean value.

Lower J_{SC} values can be attributed to lower light harvesting efficiency. As indicated in the Materials and Methods section, we use a thin and optically transparent titania layer (of only 2–3 μm in thickness) without the scattering part to allow transient absorption measurements in the transmission mode. Lower FF values are probably due to the utilization of standard commercially available titania paste without further modification and optimization for specific dye-redox mediator system (e.g., tuning the porosity). However, decent V_{OC} values matching the best reported, indicate good quality of prepared samples. To compare samples of different light harvesting efficiency in terms of the photocurrent

generation efficiency, we calculated the total absorbed photon to current efficiency (Total APCE), the parameter which is a short circuit photocurrent density corrected for the number of absorbed photons [46]. It should be also noted that our Total APCE values are quite close to the best IPCE values reported for the optimized cells (~80%), which means that the conclusions regarding electron injection dynamics should also be valid for the best performing cells with the scattering layer. We also prepared and studied the cells with MK2 dyes and $\text{Cu}^{2+}/^+(\text{tmby})_2$ redox couple, but they suffered from significantly smaller photocurrents than those of our other cells, which is presented and discussed in SI.

In order to examine the effects occurring in the solar cells upon irradiation, all characterization measurements were performed before and after continuous 30 min long irradiation at full sunlight (AM 1.5 G conditions). In Table 2, the ratios of the photovoltaic parameters measured after and before continuous irradiation lasting 30 min are given. The ratios are the averages of the three series prepared on different days, and each of the series contained at least three cells of the same type.

Table 2. The ratios of photovoltaic parameters measured after and before 30 min continuous irradiation.

Cell	PCE Ratio	Voc Ratio	FF Ratio	Jsc Ratio
Y123 $\text{Co}^{3+}/^{2+}(\text{bpy})_3$	0.99	0.96	0.98	1.04
Y123 $\text{Cu}^{2+}/^+(\text{tmby})_2$	0.81	0.96	0.82	1.03
MK2 $\text{Co}^{3+}/^{2+}(\text{bpy})_3$	1.04	0.96	1.03	1.04

The cells were irradiated in short-circuit conditions, however comparable changes were observed in open circuit conditions during our preliminary studies. Prior to the first measurements the cells were stored in the dark. A common modification observed in all studied systems is the drop in V_{OC} and rise in J_{SC} , which is a frequently observed trade-off situation occurring when the potential of the conduction band edge is shifted towards more positive values [37,38]. The above phenomenon can be explained by intercalation of lithium cations and the protons [40] present due to inevitable content of trace amounts of water in the electrolyte and mesoporous photoanode. Intercalation of both cation types to titania may be intensified by the attraction of negative charge, injected to titania when the solar cell was under irradiation. The FF changes were incoherent but implied the PCE changes.

To get a deeper insight into the reasons for photovoltaic parameters change, and to reveal the irradiation effects on the charge transfer dynamics, we will compare below the results obtained in the global analysis of TA data from the measurements performed before and after irradiation. Exemplary results for Y123 and MK2 cells are shown in Figure 4 and Supplementary Figure S6. Similarly, as in Figure 1, these figures present the pre-exponential factor spectra (wavelength-dependent amplitudes) associated with the indicated time constants obtained in the global analysis. Negative amplitudes in pre-exponential factor spectra correspond to the rise of ΔA signal (e.g., due to the rise of transient absorption bands or the recovery of the ground state of the dye or the decay of population of the transient states which emit light (stimulated emission band)), while the positive amplitudes are related to the decay of ΔA (e.g., due to the decay of population of the transient states which absorb light in the spectral range of our interest). Figure 4A,B (Y123 cells pumped at 560 nm after irradiation) should be compared with Figure 1A,B (before irradiation), Supplementary Figure S6 (Y123 cells pumped at 480 and 640 nm after irradiation) with Supplementary Figure S5 (before irradiation), and Figure 4D (MK2 cells after irradiation) with Figure 4C (before irradiation). Table 3 collects the time constants of the components presented in Figures 1 and 4.

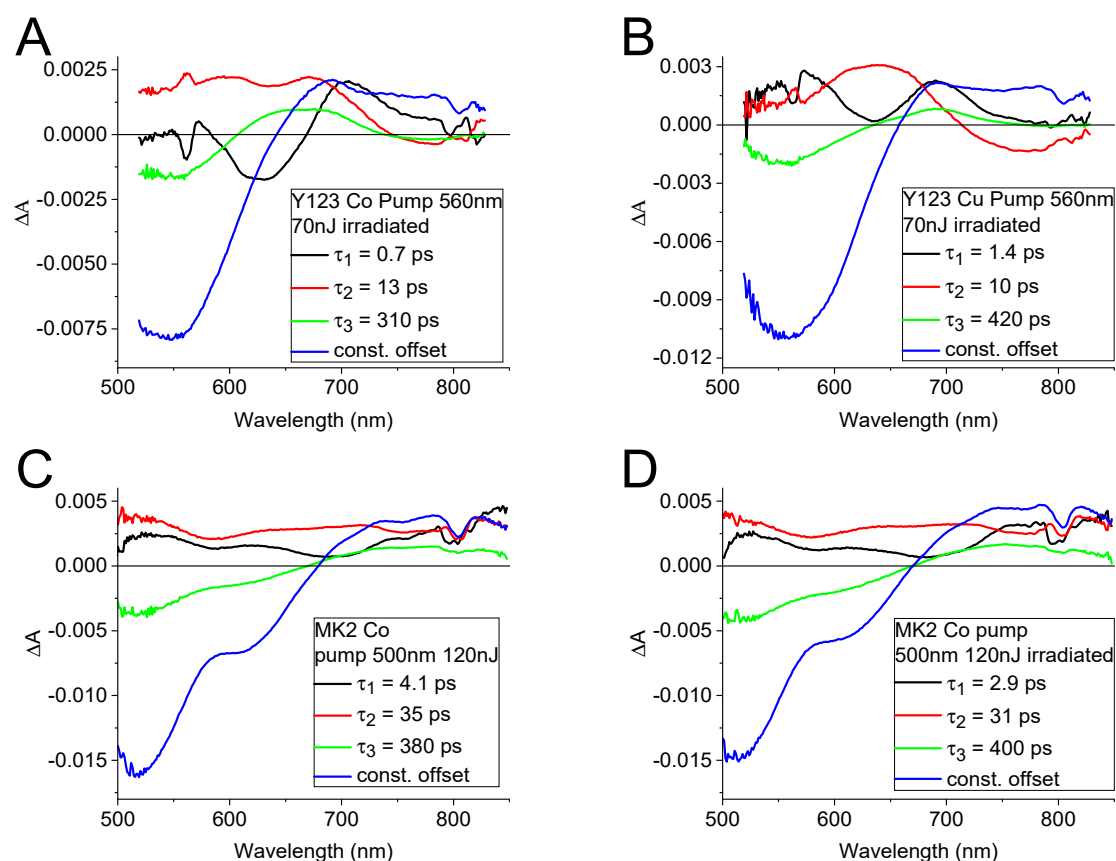


Figure 4. Results of the global analysis of transient absorption data using a three-exponential function with a constant offset for DSSC with Y123 dye and (A) cobalt- and (B) copper-based electrolyte after 30 min irradiation (compare with Figure 1) and DSSC with MK2 dye and cobalt-based electrolyte before (C) and after (D) irradiation.

Table 3. Comparison of time constants obtained in the global analysis of transient absorption measurements conducted before and after irradiation and shown in Figure 4, Supplementary Figures S5 and S6.

	Fresh			Irradiated		
	τ_1 [ps]	τ_2 [ps]	τ_3 [ps]	τ_1 [ps]	τ_2 [ps]	τ_3 [ps]
Y123 Co ^{3+/2+} (bpy) ₃ ^a	1.0	18	370	0.7	13	310
Y123 Cu ^{2+/+} (tmby) ₂ ^a	1.5	12	530	1.4	10	420
MK2 Co ^{3+/2+} (bpy) ₃ ^b	4.1	35	380	2.9	31	400

^a 560 nm excitation (480 nm and 640 nm given in Supplementary Table S1), ^b 500 nm excitation.

Our interpretation of the transient absorption measurements collected for Y123 sensitized solar cells is provided in the previous part of this paper. On the other hand, MK2 dye was extensively studied by our group and we based our interpretation on the previous reports [41–45]. Namely, we attributed the two faster (3–4 ps and 30–35 ps, black and red lines in Figure 4C,D) components to electron injection process. Similarly, as for Y123, the justification is that their pre-exponential factor spectra contain positive contributions from the decaying absorption from S₁ excited electronic state (to the higher excited electronic states of the dye) and they contain indentation originating from stimulated emission (with minima at about 700 nm for the faster component and redshifted to about 750 nm in the slower component, the latter due to thermalization of hot excited state). Slightly faster electron injection for MK2 dye relative to that for Y123 dye (the slowest component 30–35 ps for MK2 versus 80–95 ps for Y123) is probably due to the differences in the dyes structures and dye-titania electron coupling, as the difference between the dye LUMO and titania CB potentials is similar for both dyes (0.39 V for MK2 [51] and 0.44 V for Y123 [46]). The

pre-exponential factor spectra of the third component (green line in Figure 4C,D) match the spectra of constant offset constituent (blue line in Figure 4C,D, containing ground state depopulation recovery and the oxidized dye spectra decay) therefore, represent back electron transfer (recombination) from titania conduction band to the oxidized form of the MK2 dye.

The nature of the wavelength dependent pre-exponential factor spectra remains unchanged by irradiation (see Figures 1 and 4, the relative amplitudes of the pre-exponential factor spectra are similar before and after irradiation). However, clear changes in the associated time constants are observed (Figures 1 and 4, Table 3).

The fastest injection components (τ_1) recorded for the Y123 sensitized cells pumped at 560 nm are shortened: τ_1 from 1.0 ps to 0.7 ps and from 1.5 ps to 1.4 ps, while τ_2 from 18 ps to 13 ps and from 12 ps to 10 ps for cobalt- and copper-based electrolyte respectively. Therefore, the effect is more pronounced for the samples with $\text{Co}^{3+/2+}(\text{bpy})_3$. Similar acceleration of the injection process is observed for the MK2 sensitized cells (from 4.1 ps to 2.9 ps for τ_1 and from 35 ps to 31 ps for τ_2). The above effect should be attributed to the shift of the CB edge to more positive potentials, causing an increase in the driving force for electron injection. It is obviously connected with the photovoltage–photocurrent trade-off effect described earlier. It should be noted that the trends in the changes in the electron injection time constants (and also the recombination time constants discussed later) were confirmed for at least three different series of the same type of the cells prepared and measured on different days. However, the exact reductions of injection time constants were slightly different between the series.

Electron injection acceleration is unlikely to be the only cause of rise in the photocurrent density, because the quantum yield of this process should be already high enough as the internal conversion (which is the only process competing with the injection) occurs in solution on a time scale ~ 220 ps for Y123 (previous section) and ~ 500 ps for MK2) [43]. Therefore, for better understanding of the light soaking effects, the recombination processes should be considered too. For all MK2 cells, we observed slight but regular increase in the recombination time constant upon irradiation, while for Y123 cells no systematic changes in back electron transfer dynamics could be revealed (these results are consistent with the long-time scale recombination measured in inert cells and presented in Supplementary Figure S8). However, as we have shown before, the time constant of the recombination does not need to be related to the quantum yield of this unwanted process [43]. The kinetic traces at selected wavelength can better show the efficiency of electron recombination. Therefore, we took advantage of the TA kinetics at 700 nm, representing the decay of the dye's oxidized state and thereby, the CB-dye recombination for the cells comprising Y123 dye, and 750 nm for the DSSCs based on MK2 (Supplementary Figure S9). The ratio of the residual (at 3 ns time delay) and maximal signal values of the recombination kinetics (S_{RES} parameter), can be a good representation of the charge separation efficiency in a short time scale as we have shown in our previous studies of DSSCs exploiting organic sensitizers [41,43,44,46,52].

In Figure 5 we present correlations between the Total APCE (photocurrent corrected on the number of absorbed photons) and the S_{RES} parameter values. In general, we can conclude that the residual signal representing differences in charge separation efficiency is well correlated with the Total APCE. Therefore, an increase in the photocurrent upon irradiation can be directly related to the fast charge transfer dynamics that we observed in transient absorption experiment. This conclusion is coherent with our previous reports on organic sensitizers [41,43,44,46,52]. In order to get more information about the factors causing changes in the DSSCs operation upon continuous irradiation, we prepared several modified DSSCs systems based on MK2 dye (with no TBP in the electrolyte solution, with addition of co-adsorbate (CDCA) and with copper- instead of cobalt-based electrolyte).

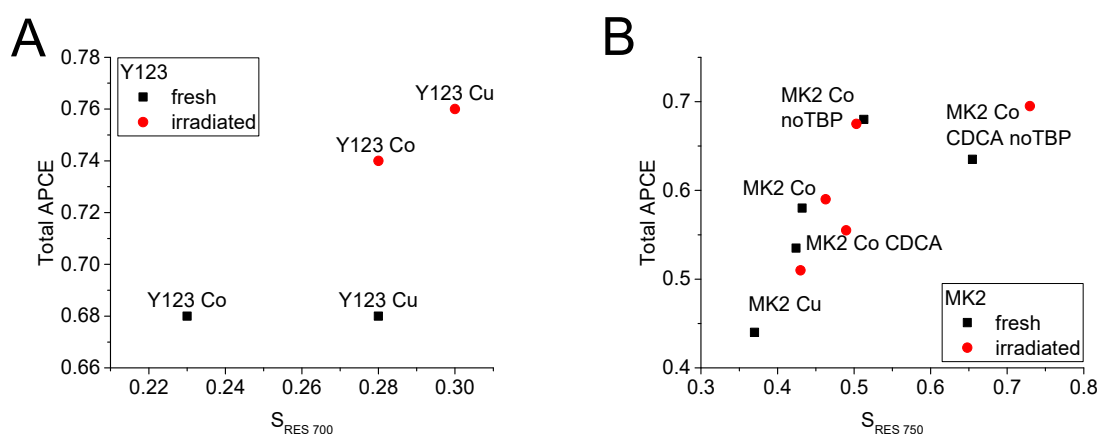


Figure 5. The correlations between Total APCE and recombinant kinetics residual signal at 700 nm for Y123 (A) and 750 nm for MK2 (B). The kinetics are given in Figure S8. Data points represent individual samples.

As mentioned before, we ascribed the effect of photocurrent enhancement to the cations of lithium and hydrogen intercalating into titania crystal lattice. Considering the shifts (correlated increase in Total APCE and S_{RES}) of the data points caused by irradiation shown in Figure 5B, we can conclude that the additives modifying the semiconductor/dye/electrolyte interface may retard the access of cations to the semiconductor's surface. Therefore, in the samples containing CDCA and/or TBP the irradiation accelerates the process of intercalation. On the other hand, it can be noticed that the sample without additives (MK2 Co noTBP) was not significantly affected by illumination. Furthermore, the Total APCE value was already relatively high, suggesting that the equilibrium was already achieved without hindrance by the additives. Another important observation is the high parallelism of the above-mentioned shifts, supporting a strong relationship between the short circuit photocurrent and the ultrafast charge separation efficiency.

4. Conclusions

In this study, we have proposed a model of charge transfer processes occurring on the dye/semiconductor interface, typical of DSSCs comprising Y123 dye and titania nanoparticle mesoporous layer. The electron injection was found to occur biphasically with the faster phase occurring within 350 fs (the resolution of mid-IR transient absorption setup) and the second one between 80 ps and 95 ps. According to the measurements performed in the visible range of detection at three different pump wavelengths, we ascribed the faster component to the injection of the electron from the hot S_1 (Frank-Condon) state and the slower constituent was assigned to the injection from the relaxed S_1 state. The contribution of the slower injection component was found to be more significant than that of the faster one, in the experiments using low pump pulse energy, and therefore it should be dominant in operational conditions.

Considering the fact that the Y123 (or its analogues) is one of the best performing sensitizers, its relatively slow electron injection should be accepted as fast enough in the absence of relevant competing deactivation processes occurring in the picosecond time scale. This should be important information for further tuning of relative excited state and CB edge energy levels, the driving force for electron injection. Despite the attempt to pump the dye in the transient absorption experiment as close as possible to the long wavelength edge of its operational spectrum, no evidence of interfacial electron transfer occurring directly from the Y123 dye's ground state to the titania conduction band was found.

In the second part of the study, we have examined the effects of illumination of the solar cells on the charge transfer rates in the Y123 sensitized solar cells and compared them with those for the systems comprising MK2 dye. The injection processes were found to be accelerated in the systems with both dyes, which was assigned to decreasing energy of the CB edge during illumination. On the other hand, the electron back transfer from

the semiconductor's conduction band to the oxidized dye was found to be slowed down in the MK2 based cells and unchanged in the systems comprising Y123. The lowering contribution of back electron transfer (estimated from the population of the oxidized dye at 3 ns) was directly correlated with the photocurrent increase upon illumination of the cells.

We believe that our efforts focused on the understanding of the electron transfer processes, occurring with involvement of Y123 dye which belongs to the most promising branch of sensitizers applied in cobalt- and copper-mediated DSSCs, will contribute to the further development of DSSC technology.

Supplementary Materials: The following are available online at <https://www.mdpi.com/1996-1073/14/2/407/s1>, Scheme S1: Molecular structures of the dyes, Scheme S2: Kinetic model for the electron injection from Y123 dye, Figure S1: Photo of the half-cell on sapphire substrate and IPCE and absorbance spectra, Figure S2: Pseudo-color 2D spectra of TA data for DSSC, Figure S3: Absorption and fluorescence spectra of the dyes solutions, Figure S4 TA data of Y123 solution, Table S1: Time constants obtained in the global analysis of TA, Figures S5 and S6: Pre-exponential factor spectra of DSSCs with Y123, Table S2: Time constants of fitted mid-IR TA kinetics, Figure S7: mid-IR control measurements, Figure S8: TA kinetics of non-irradiated/irradiated DSSCs with Y123 and MK2 and inert electrolyte, Figure S9: Kinetics of TA for Y123 and MK2 at 700 nm and 750 nm respectively Table S3: PV parameters of the cells with MK2 and Cu-based electrolyte, Figure S10: μ s-ms TA kinetics and electron lifetimes in DSSC with MK2 and Cu-based electrolyte.

Author Contributions: Conceptualization, A.G. and M.Z.; methodology, A.G. and M.Z.; validation, A.G. and M.Z.; formal analysis, A.G. and M.Z.; investigation, A.G., J.K., and M.Z.; resources, M.Z.; samples preparation, A.G.; writing—original draft preparation, A.G.; writing—review and editing, A.G., J.K., and M.Z.; visualization, A.G. and M.Z.; supervision, M.Z.; funding acquisition, M.Z. All authors have read and agreed to the published version of the manuscript.

Funding: This research was funded by NCN (National Science Centre, Poland), grant number 2015/18/E/ST4/00196.

Institutional Review Board Statement: Not applicable.

Informed Consent Statement: Not applicable.

Data Availability Statement: Not applicable.

Acknowledgments: We wish to thank Mateusz Gierszewski for kind assistance in samples preparation and Gotard Burdziński for help in nanosecond flash photolysis control measurements (Figures S8 and S10A). Our gratitude goes to Marina Freitag for the possibility of electron lifetime measurements (Figure S10B).

Conflicts of Interest: The authors declare no conflict of interest.

References

1. O'Regan, B.; Grätzel, M. A low-cost, high-efficiency solar-cell based on dye-sensitized colloidal TiO₂ films. *Nature* **1991**, *353*, 737–740. [[CrossRef](#)]
2. Kim, J.Y.; Lee, J.-W.; Jung, H.S.; Shin, H.; Park, N.-G. High-Efficiency perovskite solar cells. *Chem. Rev.* **2020**, *120*, 7867–7918. [[CrossRef](#)] [[PubMed](#)]
3. Chebrolov, V.T.; Kim, H.-J. Recent progress in quantum dot sensitized solar cells: An inclusive review of photoanode, sensitizer, electrolyte, and the counter electrode. *J. Mater. Chem.* **2019**, *7*, 4911–4933. [[CrossRef](#)]
4. Zhang, Z.; Yuan, J.; Wei, Q.; Zou, Y. Small-Molecule electron acceptors for efficient non-fullerene organic solar cells. *Front. Chem.* **2018**, *6*, 414. [[CrossRef](#)] [[PubMed](#)]
5. Michaels, H.; Rinderle, M.; Freitag, R.; Benesper, I.; Edvinsson, T.; Socher, R.; Gagliardi, A.; Freitag, M. Dye-Sensitized solar cells under ambient light powering machine learning: Towards autonomous smart sensors for the internet of things. *Chem. Sci.* **2020**, *11*, 2895–2906. [[CrossRef](#)]
6. Freitag, M.; Teuscher, J.; Saygili, Y.; Zhang, X.; Giordano, F.; Liska, P.; Hua, J.; Zakeeruddin, S.M.; Moser, J.-E.; Grätzel, M.; et al. Dye-Sensitized solar cells for efficient power generation under ambient lighting. *Nat. Photonics* **2017**, *11*, 372–378. [[CrossRef](#)]
7. Freitag, M.; Boschloo, G. The revival of dye-sensitized solar cells. *Curr. Opin. Electrochem.* **2017**, *2*, 111–119. [[CrossRef](#)]
8. Koumura, N.; Wang, Z.S.; Mori, S.; Miyashita, M.; Suzuki, E.; Hara, K. Alkyl-Functionalized organic dyes for efficient molecular photovoltaics. *J. Am. Chem. Soc.* **2006**, *128*, 14256–14257. [[CrossRef](#)]

9. Feldt, S.M.; Gibson, E.A.; Gabrielsson, E.; Sun, L.; Boschloo, G.; Hagfeldt, A. Design of organic dyes and cobalt polypyridine redox mediators for high-efficiency dye-sensitized solar cells. *J. Am. Chem. Soc.* **2010**, *132*, 16714–16724. [[CrossRef](#)]
10. Ellis, H.; Eriksson, S.K.; Feldt, S.M.; Gabrielsson, E.; Lohse, P.W.; Lindblad, R.; Sun, L.; Rensmo, H.; Boschloo, G.; Hagfeldt, A. Linker unit modification of triphenylamine-based organic dyes for efficient cobalt mediated dye-sensitized solar cells. *J. Phys. Chem.* **2013**, *117*, 21029–21036. [[CrossRef](#)]
11. Tsao, H.N.; Yi, C.; Moehl, T.; Yum, J.H.; Zakeeruddin, S.M.; Nazeeruddin, M.K.; Grätzel, M. Cyclopentadithiophene bridged donor-acceptor dyes achieve high power conversion efficiencies in dye-sensitized solar cells based on the tris-cobalt bipyridine redox couple. *ChemSusChem* **2011**, *4*, 591–594. [[CrossRef](#)] [[PubMed](#)]
12. Nazeeruddin, M.K.; Kay, A.; Rodicio, I.; Humphry-Baker, R.; Mueller, E.; Liska, P.; Vlachopoulos, N.; Graetzel, M. Conversion of light to electricity by cis-X2bis(2,2'-bipyridyl-4,4'-dicarboxylate)ruthenium(II) charge-transfer sensitizers (X = Cl-, Br-, I-, CN-, and SCN-) on nanocrystalline titanium dioxide electrodes. *J. Am. Chem. Soc.* **1993**, *115*, 6382–6390. [[CrossRef](#)]
13. Bai, Y.; Yu, Q.; Cai, N.; Wang, Y.; Zhang, M.; Wang, P. High-Efficiency organic dye-sensitized mesoscopic solar cells with a copper redox shuttle. *Chem. Commun.* **2011**, *47*, 4376–4378. [[CrossRef](#)] [[PubMed](#)]
14. Freitag, M.; Giordano, F.; Yang, W.; Pazoki, M.; Hao, Y.; Zietz, B.; Gra, M.; Hagfeldt, A.; Boschloo, G. Copper phenanthroline as a fast and high-performance redox mediator for dye-sensitized solar cells. *J. Phys. Chem.* **2016**, *120*, 9595–9603. [[CrossRef](#)]
15. Saygili, Y.; Söderberg, M.; Pellet, N.; Giordano, F.; Cao, Y.; Munoz-García, A.B.; Zakeeruddin, S.M.; Vlachopoulos, N.; Pavone, M.; Boschloo, G.; et al. Copper bipyridyl redox mediators for dye-sensitized solar cells with high photovoltage. *J. Am. Chem. Soc.* **2016**, *138*, 15087–15096. [[CrossRef](#)] [[PubMed](#)]
16. Kakiage, K.; Aoyama, Y.; Yano, T.; Oya, K.; Fujisawa, J.; Hanaya, M. Highly-Efficient dye-sensitized solar cells with collaborative sensitization by silyl-anchor and carboxy-anchor dyes. *Chem. Commun.* **2015**, *51*, 15894–15897. [[CrossRef](#)]
17. Ji, J.M.; Zhou, H.; Eom, Y.K.; Kim, C.H.; Kim, H.K. 14.2% efficiency dye-sensitized solar cells by co-sensitizing novel thieno[3,2-b]indole-based organic dyes with a promising porphyrin sensitizer. *Adv. Energy Mater.* **2020**, *10*, 1–12. [[CrossRef](#)]
18. Cao, Y.; Liu, Y.; Zakeeruddin, S.M.; Hagfeldt, A.; Grätzel, M. Direct contact of selective charge extraction layers enables high-efficiency molecular photovoltaics. *Joule* **2018**, *2*, 1108–1117. [[CrossRef](#)]
19. Michaels, H.; Benesperi, I.; Edvinsson, T.; Muñoz-García, A.B.; Pavone, M.; Boschloo, G.; Freitag, M. Copper complexes with tetradentate ligands for enhanced charge transport in dye-sensitized solar cells. *Inorganics* **2018**, *6*, 53. [[CrossRef](#)]
20. Cao, Y.; Saygili, Y.; Ummadisingu, A.; Teuscher, J.; Luo, J.; Pellet, N.; Giordano, F.; Zakeeruddin, S.M.; Moser, J.-E.; Freitag, M.; et al. 11% efficiency solid-state dye-sensitized solar cells with copper(II/I) hole transport materials. *Nat. Commun.* **2017**, *8*, 15390. [[CrossRef](#)]
21. Ghadiri, E.; Zakeeruddin, S.M.; Hagfeldt, A.; Gratzel, M.; Moser, J.E. Ultrafast charge separation dynamics in opaque, operational dye-sensitized solar cells revealed by femtosecond diffuse reflectance spectroscopy. *Sci. Rep.* **2016**, *6*, 24465. [[CrossRef](#)] [[PubMed](#)]
22. Yao, Z.; Guo, Y.; Wang, L.; Hao, Y.; Guo, Y.; Franchi, D.; Zhang, F.; Kloo, L.; Sun, L. Energy-Loss reduction as a strategy to improve the efficiency of dye-sensitized solar cells. *Sol. RRL* **2019**, *3*, 1900253. [[CrossRef](#)]
23. Zhang, W.; Wu, Y.; Bahng, H.W.; Cao, Y.; Yi, C.; Saygili, Y.; Luo, J.; Liu, Y.; Kavan, L.; Moser, J.E.; et al. Comprehensive control of voltage loss enables 11.7% efficient solid-state dye-sensitized solar cells. *Energy Environ. Sci.* **2018**, *11*, 1779–1787. [[CrossRef](#)]
24. Ren, Y.; Flores-Díaz, N.; Zhang, D.; Cao, Y.; Decoppet, J.D.; Fish, G.C.; Moser, J.E.; Zakeeruddin, S.M.; Wang, P.; Hagfeldt, A.; et al. Blue photosensitizer with copper(II/I) redox mediator for efficient and stable dye-sensitized solar cells. *Adv. Funct. Mater.* **2020**, *30*, 1–7. [[CrossRef](#)]
25. Martín, C.; Ziólek, M.; Douhal, A. Ultrafast and fast charge separation processes in real dye-sensitized solar cells. *J. Photochem. Photobiol. Photochem. Rev.* **2016**, *26*, 1–30. [[CrossRef](#)]
26. Gierszewski, M.; Grądzka, I.; Glinka, A.; Ziólek, M. Insights into the limitations of solar cells sensitized with ruthenium dyes revealed in time-resolved spectroscopy studies. *Phys. Chem. Chem. Phys.* **2017**, *19*, 20463–20473. [[CrossRef](#)] [[PubMed](#)]
27. Fujisawa, J.I. Interfacial charge-transfer transitions for direct charge-separation photovoltaics. *Energies* **2020**, *13*, 2521. [[CrossRef](#)]
28. Fujisawa, J.I.; Hanaya, M. Light harvesting and direct electron injection by interfacial charge-transfer transitions between TiO₂ and carboxy-anchor dye LEG4 in dye-sensitized solar cells. *J. Phys. Chem.* **2018**, *122*, 8–15. [[CrossRef](#)]
29. Lindström, H.; Södergren, S.; Solbrand, A.; Rensmo, H.; Hjelm, J.; Hagfeldt, A.; Lindquist, S.-E. Li⁺ ion insertion in TiO₂ (Anatase). 2. Voltammetry on nanoporous films. *J. Phys. Chem.* **1997**, *101*, 7717–7722. [[CrossRef](#)]
30. Ellingson, J.R.; Asbury, J.B.; Ferrere, S.; Ghosh, H.N.; Sprague, J.R.; Lian, T.; Nozik, A.J. Sub-Picosecond injection of electrons from excited {Ru(2,2'-bipy-4,4'-dicarboxy)₂(SCN)₂} into TiO₂ using transient mid-infrared spectroscopy. In Proceedings of the 12th International Conference on Photochemical Conversion and Storage of Solar Energy, Berlin, Germany, 9–14 August 1998.
31. Hilgendorff, M.; Sundström, V. Dynamics of electron injection and recombination of dye-sensitized TiO₂ particles. *J. Phys. Chem.* **1998**, *102*, 10505–10514. [[CrossRef](#)]
32. Durrant, J.R.; Haque, S.A.; Palomares, E. Towards optimisation of electron transfer processes in dye sensitised solar cells. *Coord. Chem. Rev.* **2004**, *248*, 1247–1257. [[CrossRef](#)]
33. Andersen, N.A.; Lian, T. Ultrafast electron transfer at the molecule-semiconductor nanoparticle interface. *Annu. Rev. Phys. Chem.* **2005**, *56*, 491–519. [[CrossRef](#)] [[PubMed](#)]
34. Ardo, S.; Meyer, G.J. Photodriven heterogeneous charge transfer with transition-metal compounds anchored to TiO₂ semiconductor surfaces. *Chem. Soc. Rev.* **2009**, *38*, 115–164. [[CrossRef](#)] [[PubMed](#)]

35. Katoh, R.; Furube, A. Electron injection efficiency in dye-sensitized solar cells. *J. Photochem. Photobiol. Photochem. Rev.* **2014**, *20*, 1–16. [[CrossRef](#)]
36. Ponseca, C.S.; Chábera, P.; Uhlig, J.; Persson, P.; Sundström, V. Ultrafast electron dynamics in solar energy conversion. *Chem. Rev.* **2017**, *117*, 10940–11024. [[CrossRef](#)]
37. Listorti, A.; Creager, C.; Sommeling, P.; Kroon, J.; Palomares, E.; Fornelli, A.; Breen, B.; Barnes, P.R.F.; Durrant, J.R.; Law, C.; et al. The mechanism behind the beneficial effect of light soaking on injection efficiency and photocurrent in dye sensitized solar cells. *Energy Environ. Sci.* **2011**, *4*, 3494–3501. [[CrossRef](#)]
38. Cabau, L.; Pellejà, L.; Clifford, J.N.; Kumar, C.V.; Palomares, E. Light soaking effects on charge recombination and device performance in dye sensitized solar cells based on indoline-cyclopentadithiophene chromophores. *J. Mater. Chem.* **2013**, *1*, 8994–9000. [[CrossRef](#)]
39. Gao, J.; El-zohry, A.M.; Trilaksana, H.; Gabrielsson, E.; Leandri, V.; Ellis, H.; Amario, L.D.; Safdari, M.; Gardner, J.M.; Andersson, G.; et al. Light-Induced interfacial dynamics dramatically improve the photocurrent in dye-sensitized solar cells: An electrolyte effect. *ACS Appl. Mater. Interfaces* **2018**, *10*, 26241–26247. [[CrossRef](#)]
40. Gao, J.; Yang, W.; El-Zohry, A.M.; Prajapati, G.K.; Fang, Y.; Dai, J.; Hao, Y.; Leandri, V.; Svensson, P.H.; Furó, I.; et al. Light-Induced electrolyte improvement in cobalt tris(bipyridine)-mediated dye-sensitized solar cells. *J. Mater. Chem.* **2019**, *7*, 19495–19505. [[CrossRef](#)]
41. Sobuś, J.; Kubicki, J.; Burdziński, G.; Ziótek, M. Carbazole dye-sensitized solar cells studied from femtoseconds to seconds—effect of additives in cobalt- and iodide-based electrolytes. *ChemSusChem* **2015**, *8*, 3118–3128. [[CrossRef](#)]
42. Sobuś, J.; Gierczyk, B.; Burdziński, G.; Jancelewicz, M.; Polanski, E.; Hagfeldt, A.; Ziótek, M. Factors affecting the performance of champion silyl-anchor carbazole dye revealed in the femtosecond to second studies of complete ADEKA-1 sensitized solar cells. *Chem. Eur. J.* **2016**, *22*, 15807–15818. [[CrossRef](#)] [[PubMed](#)]
43. Gierszewski, M.; Glinka, A.; Gradzka, I.; Jancelewicz, M.; Ziótek, M. Effects of post-assembly molecular and atomic passivation of sensitized titania surface: Dynamics of electron transfer measured from femtoseconds to seconds. *ACS Appl. Mater. Interfaces* **2017**, *9*, 17102–17114. [[CrossRef](#)] [[PubMed](#)]
44. Glinka, A.; Gierszewski, M.; Ziótek, M. Effects of aqueous electrolyte, active layer thickness and bias irradiation on charge transfer rates in solar cells sensitized with top efficient carbazole dyes. *J. Phys. Chem.* **2018**, *122*, 8147–8158. [[CrossRef](#)]
45. Pydzińska-Białek, K.; Glinka, A.; Drushliak, V.; Nowaczyk, G.; Florczak, P.; Ziótek, M. Impact of improvements in mesoporous titania layers on ultrafast electron transfer dynamics in perovskite and dye-sensitized solar cells. *Phys. Chem. Chem. Phys.* **2020**, *22*, 21947–21960. [[CrossRef](#)] [[PubMed](#)]
46. Glinka, A.; Gierszewski, M.; Gierczyk, B.; Burdziński, G.; Michaels, H.; Freitag, M.; Ziótek, M. Interface modification and exceptionally fast regeneration in copper mediated solar cells sensitized with indoline dyes. *J. Phys. Chem.* **2020**, *124*, 2895–2906. [[CrossRef](#)]
47. Idígoras, J.; Burdziński, G.; Karolczak, J.; Kubicki, J.; Oskam, G.; Anta, J.A.; Ziótek, M. The impact of the electrical nature of the metal oxide on the performance in dye-sensitized solar cells: New look at old paradigms. *J. Phys. Chem.* **2015**, *119*, 3931–3944. [[CrossRef](#)]
48. Haque, S.A.; Tachibana, Y.; Willis, R.L.; Moser, J.E.; Grätzel, M.; Klug, D.R.; Durrant, J.R. Parameters influencing charge recombination kinetics in dye-sensitized nanocrystalline titanium dioxide films. *J. Phys. Chem.* **2000**, *104*, 538–547. [[CrossRef](#)]
49. Nelson, J.; Haque, S.A.; Klug, D.R.; Durrant, J.R. Trap-Limited recombination in dye-sensitized nanocrystalline metal oxide electrodes. *Phys. Rev.* **2001**, *63*, 205321. [[CrossRef](#)]
50. Xiang, W.; Huang, W.; Bach, U.; Spiccia, L. Stable high efficiency dye-sensitized solar cells based on a cobalt polymer gel electrolyte. *Chem. Commun.* **2013**, *49*, 8997–8999. [[CrossRef](#)]
51. Wang, Z.S.; Koumura, N.; Cui, Y.; Takahashi, M.; Sekiguchi, H.; Mori, A.; Kubo, T.; Furube, A.; Hara, K. Hexylthiophene-Functionalized carbazole dyes for efficient molecular photovoltaics: Tuning of solar-cell performance by structural modification. *Chem. Mater.* **2008**, *20*, 3993–4003. [[CrossRef](#)]
52. Gierszewski, M.; Glinka, A.; Gradzka, I.; Gierczyk, B.; Ziótek, M. Testing new concepts in solar cells sensitized with indoline dyes—Alkoxysilyl anchoring group, molecular capping, and cobalt-based electrolyte. *J. Phys. Chem.* **2018**, *122*, 25764–25775. [[CrossRef](#)]